Electronic Supplementary Material (ESI) for Chemical Communications

A simple new competition assay for heparin binding in serum applied to multivalent PAMAM dendrimers

Stephen M. Bromfield,[a] Paola Posocco,[b] Maurizio Fermeglia,[b] Sabrina Pricl[b,c] Julián Rodríguez-López,[d] and David K. Smith*[a]

a: Department of Chemistry, University of York, Heslington, York, YO10 5DD, UK

b: Molecular Simulation Engineering (MOSE) Laboratory, Department of Engineering and Architecture (DEA), University of Trieste, 34127 Trieste, Italy.

c: National Interuniversity Consortium for Material Science and Technology (INSTM), Research Unit MOSE-DEA, University of Trieste, 34127 Trieste, Italy

d: Área de Química Orgánica, Facultad de Ciencias y Tecnologías Químicas, Universidad de Castilla la Mancha, 13071 Ciudad Real, Spain

SUPPORTING INFORMATION

Contents

1 Synthetic Methods and Characterisation Data

2 Assay Methods

3 Binding Data

4 Computational Methods

5 References

1 Synthetic Methods and Characterisation Data

Mallard Blue was synthesised as fully described in our recent paper.[1]

PAMAM dendrimers were purchased from Dendritech. Figure S1 shows the chemical structure of G2-PAMAM.

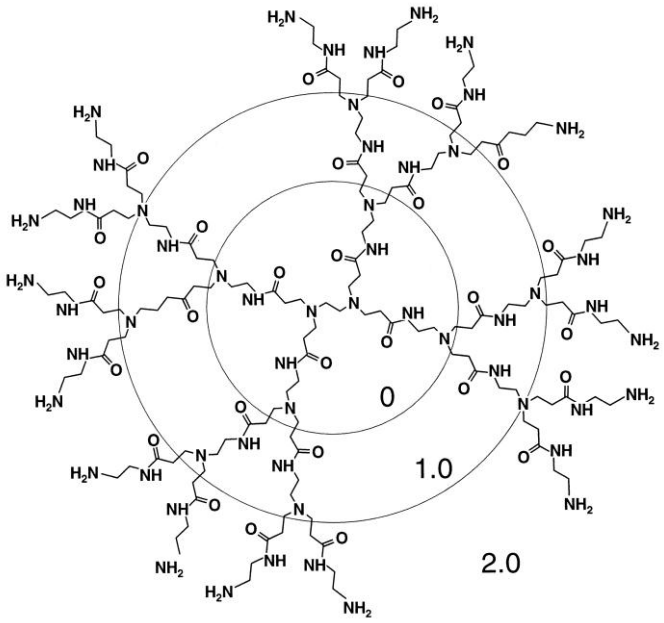

Figure S1 – Structure of G2-PAMAM

2 Assay Methods

Assay Materials. All materials, except Mallard Blue (MalB), employed in heparin binding assays were obtained from commercial sources and used without further purification. Sodium salt heparin from porcine intestinal mucosa with a molecular weight between 15,000 ± 2,000 Da (1 KU = 1000 units) was obtained from Calbiochem®. Protamine sulfate salt from salmon (Grade X, amorphous powder), PAMAM dendrimers, Trizma® hydrochloride (Tris HCl) and Human Serum (from human male AB plasma) were obtained from Sigma Aldrich. UV/Vis absorbance was measured on a Shimadzu UV-2401PC spectrophotometer.

All MalB solutions were incubated at 50°C for 24 hours prior to use and stored in the dark. All experiments were performed in triplicate.

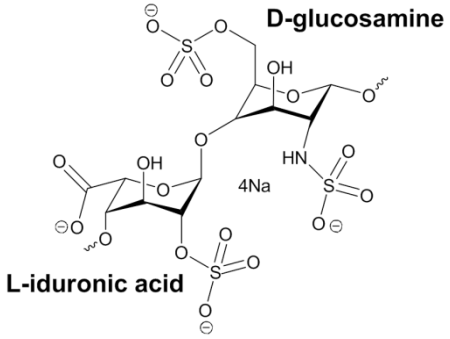

Figure S2 – Most prevalent disaccharide repeat unit in heparin chain.

For the purpose of calculations, the molecular weight of heparin is assumed as that of the sodiated analogue of the heparin repeat unit shown in Figure S2: namely 665.40 g mol^{-1}. It should be noted that as supplied, heparin only contains ca. 30-40% of material with the active sequence of repeat units. However, all of the sample contains anionic saccharide units which can bind, even if they are in the wrong sequence. Hence to best evaluate binding concentrations and charge efficiencies, we report the total concentration of the anionic disaccharide – irrespective of whether it is present in the active form of heparin or not. However, all presented data which refers to the 'dose' of binders (in mg/units) refers to their ability to bind only the specific clinically active heparin.

Heparin Displacement Assay In Buffer. A cuvette containing 2 mL of MalB (25 μM), heparin (27 μM) and NaCl (150 mM) in Tris HCl (10 mM) was titrated with binder stock solution to give the cuvette a suitable binder-heparin charge ratio. The binder stock solution was composed of the original MalB/heparin/NaCl/Tris HCl stock solution endowed additionally with a concentration of binder such that, after addition of 10 μL binder stock, the cuvette charge ratio (+ : –) is 0.1. After each addition, the cuvette was inverted to ensure good mixing and the absorbance at 615 nm was recorded against a Tris HCl (10 mM) baseline. Absorbance was normalised between a solution of MalB (25 μM), NaCl (150 mM) in Tris HCl (10 mM) and one containing MalB (25 μM), heparin (27 μM), NaCl (150 mM) in Tris HCl (10 mM).

Heparin Displacement Assay In Serum. Fourteen cuvettes were charged with 1.75 mL of MalB (28.53 μM) in Tris HCl (10 mM) and a volume of binder stock solution to give the cuvette a suitable binder-heparin charge ratio. The binder stock solution was additionally endowed with its own MalB (25 μM), heparin (27 μM) and Tris HCl (10 mM) concentrations. The concentration of binder in the binder stock was determined in the same manner described for the heparin displacement assay in buffer. Separately, a heparin (216 μM) solution was made in 100% human serum. Sequentially, each cuvette was titrated with 0.25 mL of the heparin-in-serum solution and inverted to ensure thorough mixing. The absorbance was recorded at 615 nm against a baseline of (1.75 mL 10 mM Tris HCl, 0.25 mL 100% Human Serum) and normalised between a solution containing exclusively MalB (25 μM) and one containing MalB (25 μM) and heparin (27 μM).

3 Binding Data

Binding of Protamine to Heparin. Figure S3 presents the ability of protamine to displace Mallard Blue from its complex with heparin. The continued increase above normalised absorbance of 1 in the presence of serum is an effect of the increased turbidity caused by the presence of heparin-protamine aggregates.

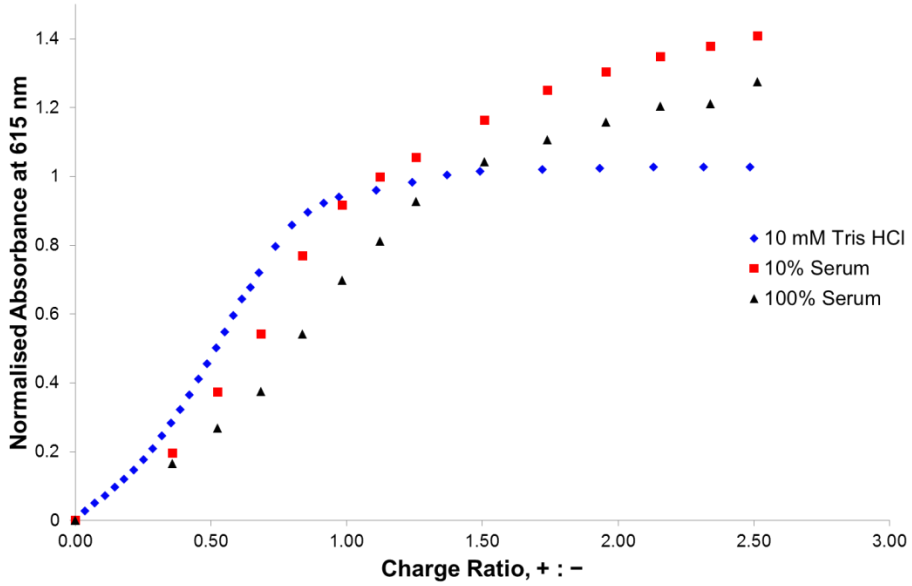

Figure S3 – Binding curves for protamine (i) blue diamonds: in Tris HCl (10 mM) and NaCl (150 mM); (ii) red squares: in Tris HCl (10 mM) with heparin delivered in 10% Serum; (iii) black triangles: in Tris HCl (10 mM) with heparin delivered in 100% Serum.

Binding of PAMAM Dendrimers to Heparin. Figure S4 shows the binding curves for G0-PAMAM, G2-PAMAM, G4-PAMAM and G6-PAMAM in the MalB displacement assay. In general, with the exception of G0-PAMAM which is unable to bind heparin, as the PAMAM dendrimers becomes larger, they become less efficient at using their charge for binding to the heparin. As such G2-PAMAM is the most effective heparin binding system.

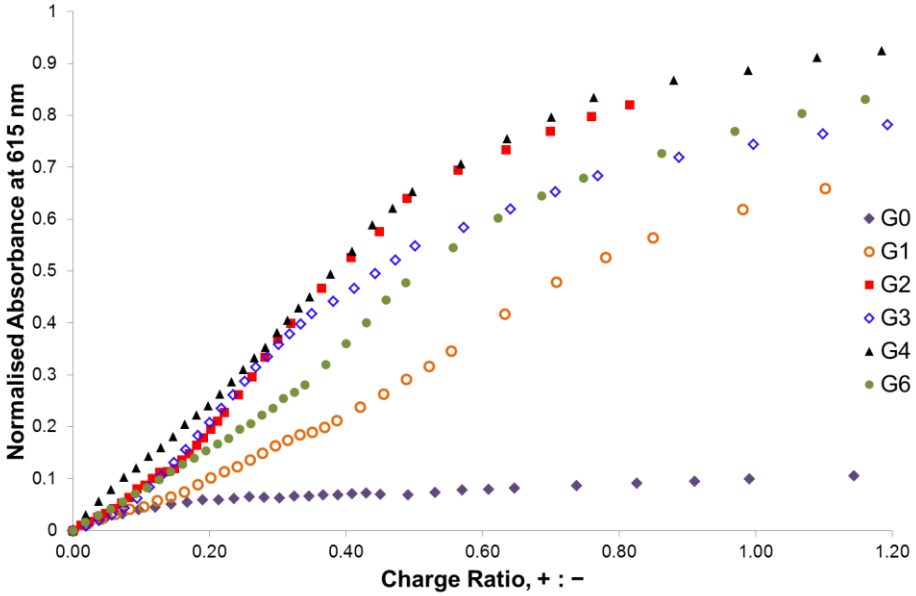

Figure S4 – Heparin binding curves in NaCl (150 mM) and Tris HCl (10 mM) for (i) purple diamonds: G0-PAMAM; (ii) orange open circles: G1-PAMAM; (iii) red squares: G2-PAMAM; (iv) blue open diamonds: G3-PAMAM; (v) black triangles: G4-PAMAM; (vi) green circles: G6-PAMAM.

Figure S5 shows the binding curves for G2-PAMAM in NaCl (150 mM) / Tris HCl (10 mM) system and that with the heparin delivered in 100% Human Serum. The continued increase above normalised absorbance of 1 in the presence of serum is an effect of the increased turbidity caused by the presence of heparin-protamine aggregates.

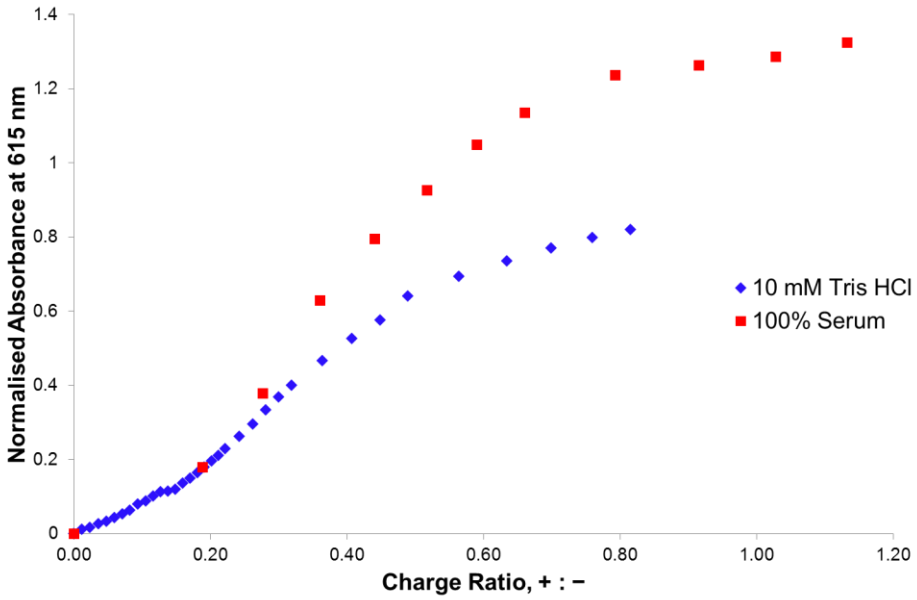

Figure S5 – Heparin binding curves for G2-PAMAM (i) blue diamonds: with heparin (27 μM), NaCl (150 mM) in Tris HCl (10 mM); (ii) red squares: in Tris HCl (10 mM) with heparin delivered in 100% Human Serum.

4 Computational Methods

Protamine modelling. The three-dimensional (3D) structure of a representative protamine model (main text, Figure 1) was built by a cascade sequence of secondary structure predictions (SSPs) and homology modeling (HM) techniques. The SSPs were carried out using the following prediction servers PSIPRED (http://bioinf.cs.ucl.ac.uk/psipred/),[2] DISOPRED2 (http://bioinf.cs.ucl.ac.uk/disopred/),[3] Predict Protein (http://www.predictprotein.org/),[4] I-TASSER (http://zhanglab.ccmb.med.umich.edu/I-TASSER/),[5] and the Secondary Structure Prediction tool of the *Discovery Studio* (*DS*) platform (v. 2.1, Accelrys, San Diego, CA, USA) in a comparative fashion.

All SSP outputs were compared for quality, reliability, and matching. As expected, utterly similar results were obtained, according to which the protamine secondary structure should feature, aside some loops, two major α-helical domains, as shown in Figure S6 for the PSIPRED SSP as an example.

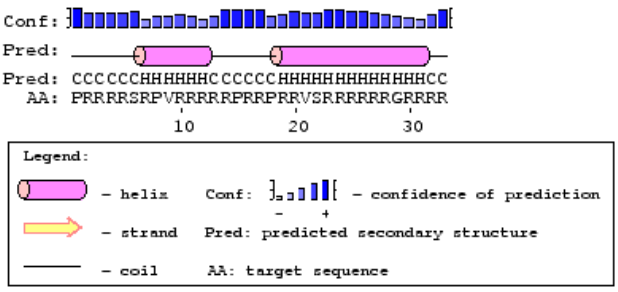

Figure S6 – General secondary structure prediction of the idealized protamine chain as obtained from PSIPRED.

The corresponding 3D model of protamine was built *de novo* using a consolidated procedure[6] based on a combination of the *Build and Edit Protein* modulus of *DS* and of the MODELER suite (http://salilab.org/modeller/).[7] All generated models were checked and ranked for quality coupling conformational (i.e., Ramachandran plot) and energetic criteria (i.e., energy minimization using the *DS* CHARMM program[8]); and the best ranked solution according to both criteria within the entire set of generated models was finally selected. The resulting

structure was further adjusted manually to fully match the results of secondary structure predictions and optimized for side chain conformation.

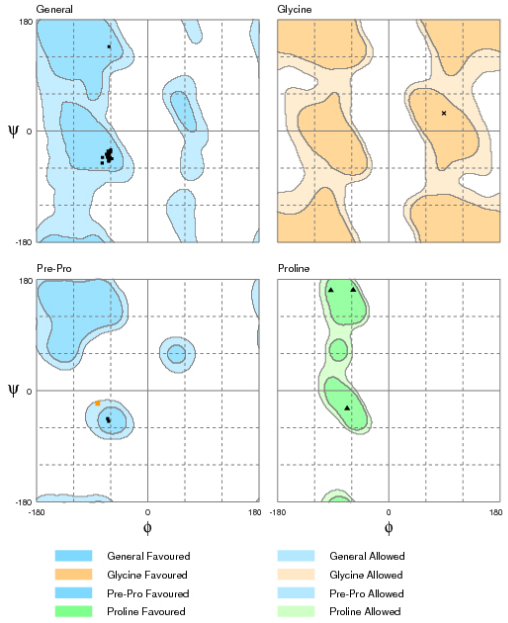

Figure S7 – Ramachandran plot of the 3D protamine model.

The stereochemistry quality of the resulting model was checked using PROCHECK,[9] WHATIF,[10] and ProSA (https://prosa.services.came.sbg.ac.at/prosa.php).[11] The analysis of the Ramachandran plot produced by PROCHECK of the main torsional angles of the preliminary model revealed that a total of 96.6% of the protein residues (32/33) were in the most favoured regions of the plot, with 3.4% (1/33) in additionally allowed regions, giving a total of 100.0% (see Figure S7). Bond lengths and angles were all found to be within their normal range, and no bumps (corresponding to high van der Waals energies) were detected. Other stereochemical parameters, such as peptide planarity, bad non-bonded interactions, main-chain hydrogen bonding energy, and standard deviations of χ_1 angle (i.e., the first torsion angle of the side chains) were also examined and checked for validity. Accordingly, the total quality G-factor was – 0.15, revealing the good quality of the 3D protamine model structure since reasonable values for the G-factor in PROCHECK fall between 0 and – 0.5, with the best models displaying values closest to 0. The packing quality of the 3D model was assessed for the absence of steric clashes between any pair of atoms. The results of the WHATIF quality report showed a normality index (z-score) of -0.766, a good value which falls in the acceptable range for a valid structure (z-score > -5.0). The analysis of the ProSA

results revealed that the residue-residue interaction energies were all attractive, indicating no bad backbone contacts for the present model. Lastly, the good overall quality of the 3D protamine model was also reflected in the corresponding value of the ProSA normalized z-score = 1.12, being z-score > 0.70 indicative of a good structure.

The preliminary 3D model of protamine was further refined and its stability verified via a cycle of molecular dynamics (MD) simulations in a solvated environment. All MD simulations were carried out using the *Sander* and *Pmemd* modules of the AMBER 11 suite of programs.[12] Accordingly, protamine was solvated by a TIP3P[13] box of water extending at least 10.0 Å in each direction from the solute; then, a suitable number of Cl^- and Na^+ counterions were added to ensure the overall charge neutrality of the system and to mimic a physiological ionic strength of 0.15 M. The energy of the resulting system was relaxed via a multi-step minimization procedure using the AMBER *ff03* force field,[14] as follows. First only the water molecules and counterions were minimized for 5000 cycles of steepest-descent minimization. Next, also the side chains of protamine were further relaxed using a 1000-cycle energy minimization to relieve possible unexpected side-chain clashes. Lastly, the whole system was energy relaxed for further 1000-cycles of conjugate-gradient minimization. The system was then gradually heated to T = 300 K in three constant temperature/constant volume (NVT) MD intervals, allowing a 20 ps interval per each 100 K, followed by constant temperature/constant pressure (NPT) MD simulations at 300 K for other 60 ps with the backbone of protamine restrained with an harmonic potential, while all water molecules, counterions, and the protamine side chains were allowed to move. Then, the whole system was further equilibrated in the NVT ensemble for 15 ns at 300 K, to attain a well relaxed protamine structure and to verify the stability of the corresponding MD trajectory. The time step used in the MD simulation was 2 fs. Periodic boundary conditions were used with Berendsen temperature coupling[15] and P =1 atm, with isotropic molecule-based scaling. The SHAKE algorithm[16] was used to fix all covalent bonds containing hydrogen atoms. Long-range nonbonded van der Waals interactions were truncated by using a dual cut off of 6 and 12 Å, respectively, where energies and forces due to interactions between 6 and 12 Å were updated every 20 time steps. The particle mesh Ewald method[17] was used to treat the long-range electrostatics. A residue-based cut off of 8 Å was used for the non-covalent interactions. During the NVT MD simulations, the coordinates of protamine were saved every 1 ps.

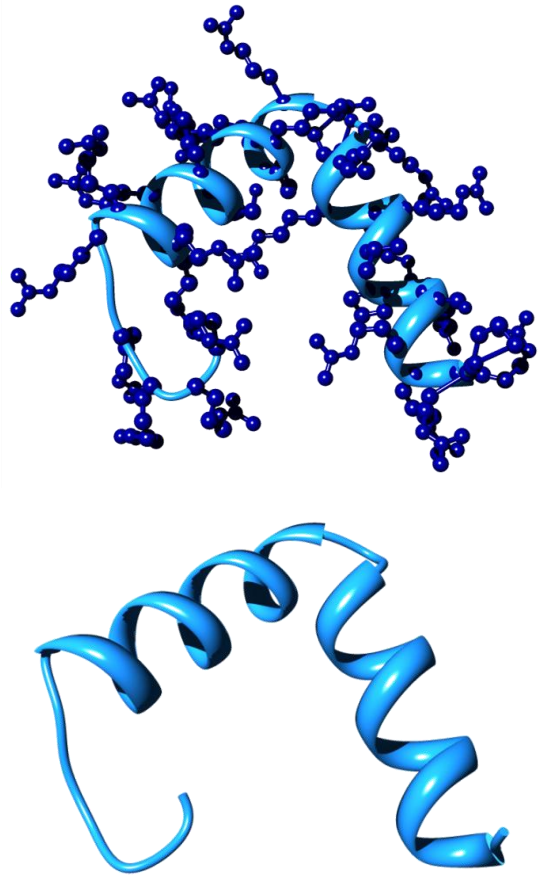

Figure S8 – Representations of the 3D structure of the representative protamine model (main text, Figure 1). Water molecule, ions and counterions are omitted for clarity.

The 3D protamine model structure remained stable for all 15 ns of the MD trajectory, as indicated by the small fluctuations of the root-mean-square (RMS) deviation of the simulated position of the backbone atoms with respect to those of the initial structure and the corresponding total potential energy of the system (data not shown). From the above described 15 ns equilibrated MD trajectory, the protamine coordinates were extracted from last frame of the equilibrium MD trajectory, and the corresponding 3D protamine model was further evaluated for quality and reliability. By comparison with the pre-refined structure, the G-factor increased from -0.15 to -0.10, indicating that the MD simulations further optimized the contacts between nonbonded atoms without increasing the number of bad dihedral angles of the structure. The result of the ϕ-ψ combination displayed by the Ramachandran plot of the MD protamine relaxed model is identical to that shown in Figure S8, validating both the quality and the stability of the initial model. Other stereochemical parameters such as dihedral angles, covalent geometry, and planarity were also examined. The respective G-factor were all close to zero, and all values were well within the acceptable limits. As

expected, the atomic contact analysis of WHATIF and the value of the PROSA normalized z-score were practically identical to those of the initial model, ultimately confirming the final good quality of the 3D protamine molecule shown in Figure S8.

Heparin modelling. A representative heparin chain (molecular weight ≅ 15,000 Da, 23 disaccharide repeating units) was built from the recently determined, high resolution NMR heparin structures in solution.[18] In particular, the present chain was initially build by joining a heparin chain of 18 disaccharide repeating units (3IRL.pdb) with one of 15 disaccharide repeating units (3IRK.pdb) using *DS*. The resulting heparin chain was then immersed in a box of TIP3P[12] water molecules, and the correct number of Cl^- and Na^+ counterions were added to neutralize the systems and generate the physiological ionic strength of 0.15 M. The solvated heparin system was then equilibrated following the sequence of energy minimization and MD simulation procedure described above for protamine; in this case, the Amber/Glycam06 force field[19] was used in all simulations.

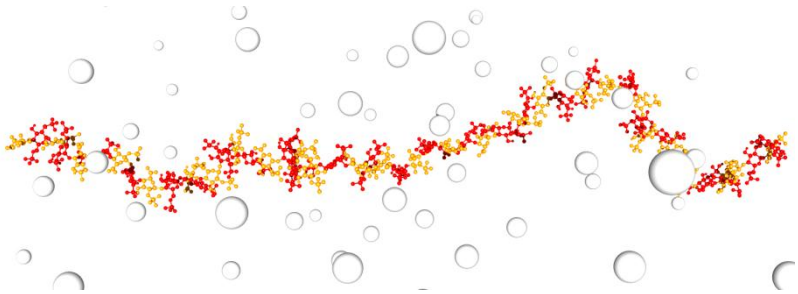

Figure S9 – MD equilibrated snapshots the representative heparin chain. Color legend: dark red, D-glucosamine units, orange, L-iduronic acid units. Some representative Cl^- and Na^+ ions are shown as large and small white spheres, respectively. Water omitted for clarity.

The optimized model of the representative heparin chain is shown in Figure S9. The resulting structure is characterized by the following average values of the φ and ψ angles of α-L-iduronic acid (IdoA) and N-sulfated glucosamine (GlcNS) (Figure S1), as obtained from the corresponding MD trajectory: φ = - 55° ± 26° and ψ = 132° ± 27° for IdoA-GlcNS, and φ = 118° ± 23° and ψ = 86° ± 20° for GlcNS-IdoA, respectively. These values are in agreement with those determined recently by synchrotron X-ray solution scattering on heparin chains of similar length.[18]

Modelling of PAMAM dendrimers. The optimized model of all ethylenediamine (EDA) PAMAM dendrimers generations considered in this study were taken from our previous work.[20]

Complexation of heparin with G1-G4, and G6 PAMAM dendrimers and protamine. The complex of heparin with all PAMAM dendrimer generations considered in this work was achieved by adapting a consolidated procedure developed by our group.[20,21] Accordingly, it will be reported here briefly. To build the 3D models of the heparin/dendrimer complexes, the heparin chain was initially placed close to each dendrimer periphery. The resulting molecular pair was subsequently energy minimized to yield a starting structure devoid of substantial van der Waals overlaps. Each single dendrimer molecule as well as the corresponding heparin complexes were then solvated with an appropriate number of TIP3P[13] water molecules extending at least 20 Å from the solute. A suitable number of Na^+ and Cl^- counterions were added to neutralize the system and to mimic an ionic strength level of 0.15 M. Eventual overlapping water molecules were removed. Each complex molecular model was then subjected to a combination of steepest descent and conjugate gradient energy minimization steps (50000 cycles), in order to relax close atomic distances. The energy-minimized systems were further equilibrated by performing 4 to 12 ns MD simulations in the NPT ensemble using an integration step of 1fs. During equilibration, different energetic components as well as static and conformational properties (e.g., radius of gyration of the dendrimer, average distance between the dendrimer and the heparin molecule, and distribution of ions and water molecules around the complex) were monitored, to ensure their stabilization prior to production runs. MD production runs were performed on equilibrated systems again in the NPT ensemble with 1 fs time step (T = 300 K, P = 1 bar). The Langevin method for the control of temperature (with a damping coefficient of 5 ps^{-1}) and the Nose-Hoover Langevin piston method[22] for the control of pressure (using a piston period of 0.8 ps and a decay time of 0.4 ps) were employed for temperature and pressure control, respectively. Electrostatic interactions were computed by means of the particle mesh Ewald (PME) algorithm[17]. Depending on the molecular dimensions of the examined systems, production MD trajectories of 10 to 50 ns were generated. The overall lengths of the trajectories thus produced were sufficient to achieve the complete decay of the global conformational relaxation of the dendritic component, as expressed by the autocorrelation function of the squared fluctuations of its radius of gyration (data not shown). The binding of protamine to heparin was modelled in an analogous manner

Determination of the binding free energy of protamine and G1-G4 & G6 PAMAM dendrimers and heparin. To estimate the free energy of binding ΔG_{bind} between each dendrimer generation (and protamine) and the heparin molecule, we resorted to a well-established computational recipe[21] based on the so-called Molecular Mechanics/Poisson-Boltzmann Surface Area (MM/PBSA) methodology.[23] Briefly, for a non-covalent association of two molecular entities A + B → AB, the free energy of binding involved in the process may be generally written as $\Delta G_{bind} = G_{AB} - G_A - G_B$. For any species on the right hand side of this equation, from basic thermodynamics we have $G_i = H_i - TS_i$, where H_i and S_i are the enthalpy and entropy of the i-th species, respectively and T is the absolute temperature. In view of this expression, ΔG_{bind} can then be written as: $\Delta G_{bind} = \Delta H_{bind} - T\Delta S_{bind}$. ΔH_{bind} is the variation in enthalpy upon association and, in the MM/PBSA framework of theory, can be calculated by summing the molecular mechanics energies (ΔE_{MM}) and the solvation free energy (ΔG_{solv}), i.e., $\Delta H_{bind} = \Delta E_{MM} + \Delta G_{solv}$. ΔE_{MM} in turn is obtained from a single MD trajectory of the molecular complex as $\Delta E_{MM} = \Delta E_{vdW} + \Delta E_{ele}$, where ΔE_{vdW} is the variation of the nonbonded van der Waals energy and ΔE_{ele} is the electrostatic contribution calculated from the Coulomb potential. The solvation term ΔG_{solv} is given by $\Delta G_{solv} = \Delta G_{pol} + \Delta G_{np}$, in which ΔG_{pol} is obtained by solving the Poisson-Boltzmann equation and ΔG_{np} is the nonpolar solvation term estimated via the semiempirical expression: $\Delta G_{np} = \gamma \times SASA + \beta$, in which SASA is the solvent accessible surface area of the molecule, γ is the surface tension parameter (0.00542 kcal/Å^2/mol), and β = 0.92 kcal/mol. Finally, the estimation of the entropic contribution $-T\Delta S_{bind}$ is performed using normal mode analysis, which requires the computation of eigenvectors and eigenvalues via the diagonalization of the Hessian matrix.

Finally, the effective number of charges involved in binding, and the corresponding effective free energy of binding values (main text, Table 2) were obtained performing a *per residue binding free energy decomposition* (PRBFED) exploiting the MD trajectory of each given heparin/dendrimer (protamine) complex. This analysis was carried out using the MM/GBSA approach,[24] and was based on the same snapshots used in the binding free energy calculation.

General modeling information. All MD-based simulations were carried out using the *Sander* and *Pmemd* modules of AMBER 11,[12] running in parallel on 256 processors of the

IBM PLX-GPU calculation cluster of the CINECA supercomputer facility (Bologna, Italy). The entire computational procedure was optimized by integrating AMBER 11 in modeFRONTIER, a multidisciplinary and multi-objective optimization and design environment.

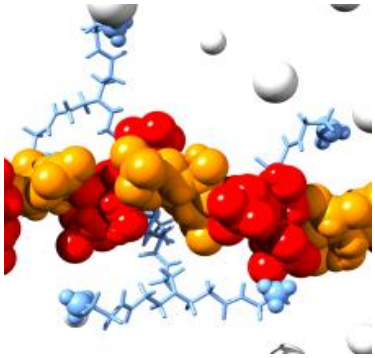

Figure S10 – Equilibrated MD snapshots of G1-PAMAM bound to heparin. Heparin, dark red D-glucosamine and orange L-iduronic acid CPK spheres. Some Cl^- and Na^+ ions are shown as large and small white spheres.

5 References

1. S. M. Bromfield, A. Barnard, P. Posocco, M. Fermeglia, S. Pricl and D. K. Smith, *J. Am. Chem. Soc.* 2013, **135**, 2911-2914.
2. L. J. McGuffin, K. Bryson, and D. T. Jones, *Bioinformatics* 2000, **16**, 404-405.
3. J. J. Ward, J. S. Sodhi, L. J. McGuffin, B. F. Buxton and D. T. Jones, *J. Mol. Biol.* 2004, **337**, 635-645.
4. B. Rost, G. Yachdav and J. Liu, *Nucleic Acids Res*. 2004, **32**, 321-326.
5. R. Ambrish, K. Alper and Z. Yang, *Nat. Protoc*. 2010, **5**, 725-738.
6. (*a*) E. Laurini, V. Dal Col, M. G. Mamolo, D. Zampieri, P. Posocco, M. Fermeglia, L. Vio and S. Pricl, *ACS Med. Chem. Lett.* 2011, **2**, 834-839; (*b*) A. Carta, I. Briguglio, S. Piras, G. Boatto, P. La Colla, R. Loddo, M. Tolomeo, S. Grimaudo, A. Di Cristina, R. M. Pipitone, E. Laurini, M. S. Paneni, P. Posocco, M. Fermeglia and S. Pricl, *Eur. J. Med. Chem*. 2011, **46**, 4151-4167; (*c*) P. Dileo, S. Pricl, E. Tamborini, T. Negri, S. Stacchiotti, A. Gronchi, P. Posocco, E. Laurini, P. Coco, E. Fumagalli, P. G. Casali and S. Pilotti, *Int. J. Cancer* 2011, **128**, 983-990; (*d*) A. Carta, M. Loriga, S. Piras, G. Paglietti, M.

Ferrone, M. Fermeglia, S. Pricl, P. La Colla, G. Collu, T. Sanna and R. Loddo, *Med. Chem*. 2007, **3**, 520-532.

7. (*a*) N. Eswar, M. A. Marti-Renom, B. Webb, M. S. Madhusudhan, D. Eramian, M. Shen, U. Pieper and A. Sali, *Current Protocols in Bioinformatics*, John Wiley & Sons, Inc., Supplement 2006, 15, 5.6.1-5.6.30; (*b*) M. A. Marti-Renom, A. Stuart, A. Fiser, R. Sánchez, F. Melo and A. Sali, *Annu. Rev. Biophys. Biomol. Struct*. 2000, **29**, 291-325; (*c*) A. Sali and T. L. Blundell, *J. Mol. Biol*. 1993, **234**, 779-815; (*d*) A. Fiser, R. K. Do and A. Sali, *Prot. Sci.* 2000, **9**, 1753-1773.
8. B. R. Brooks, C. L. Brooks, A. D. Mackerell, L. Nilsson, R. J. Petrella, B. Roux, Y. Won, G. Archontis, C. Bartels, S. Boresch A. Caflisch, L. Caves, Q. Cui, A. R. Dinner, M. Feig, S. Fischer, J. Gao, M. Hodoscek, W. Im, K. Kuczera, T. Lazaridis, J. Ma, V. Ovchinnikov, E. Paci, R. W. Pastor, C. B. Post, J. Z. Pu, M. Schaefer, B. Tidor, R. M. Venable, H. L. Woodcock, X. Wu, W. Yang, D. M. York and M. Karplus, *J. Comp. Chem*. 2009, **30**, 1545-1615.
9. R. A. Laskowski, M. W. MacArthur, D. S. Moss and J. M. Thornton, *J. Appl. Cryst*. 1993, **26**, 283-291.
10. G. Vriend, *J. Mol. Graph*. 1990, **8**, 52-56 (1990).
11. M. Wiederstein and M. J. Sippl, *Nucleic Acid Res*. 2007, **35**, W407-W410.
12. D. A. Case *et al*, AMBER 11, University of California, San Francisco, USA, 2010.
13. W. L. Jorgensen, J. Chandrasekhar, J. D. Madura, R. W. Impey and M. L. Klein, *J. Chem. Phys*. 1983, **79**, 926-935.
14. Y. Duan C. Wu S. Chowdhury M. C. Lee G. Xiong W. Zhang R. Yang P. Cieplak R. Luo T. Lee J. Caldwell, J. Wang and P. A. Kollman *J. Comput. Chem*. 2003, **24**, 1999-2012.
15. H. J. C. Berendsen, J. P. M. Postma, W. F. Van Gunsteren, A. DiNola and J. R. Haak, *J. Chem. Phys*. 1984, **81**, 3684-3690.
16. J. P. Ryckaert, G. Ciccotti and H. J. C. Berendsen, *J. Comput. Phys.* 1977, **23**, 327-341.
17. A. Toukmaji, C. Sagui, J. Board and T. Darden, *J. Chem. Phys*. 2000, **113**, 10913-10927.
18. S. Khan, J. Gor, B. Mulloy and S. J. Perkins, *J. Mol. Biol*. 2010, **5**, 504-521.
19. K. N. Kirschner, A. B. Yongye, S. M. Tschampel, C. R. Daniels, B. L. Foley and R. J. Woods, *J. Comput. Chem*. 2008, **29**, 622-655.
20. G. M. Pavan, P. Posocco, A. Tagliabue, M. Maly, A. Malek, A. Danani, E. Ragg, C. V. Catapano and S. Pricl, *Chem. Eur. J*. 2010, **16**, 7781-7795.
21. (*a*) X. Liu, C. Liu, E. Laurini, P. Posocco, S. Pricl, F. Qu, P. Rocchi and L. Peng, *Mol. Pharm*. 2012, **9**, 470-481; (*b*) K. Karatasos, P. Posocco, E. Laurini and S. Pricl,

Macromol Biosci. 2012, **12**, 225-240; (*c*) X. Liu, J. Wu, M. Yammine, J. Zhou, P. Posocco, S. Viel, C. Liu, F. Ziarelli, M. Fermeglia, S. Pricl, G. Victorero, C. Nguyen, P. Erbacher, J.-P. Behr and L. Peng, *Bioconjugate Chem*. 2011, **22**, 2461-2473; (*d*) A. Barnard, P. Posocco, S. Pricl, M. Calderon, R. Haag, M. E. Hwang, V. T. Shum, D. W. Pack and D. K. Smith, *J. Am. Chem. Soc*. 2011, **133**, 20288-20300; (*e*) S. P. Jones, N. P. Gabrielson, C.-H. Wong, H.-F. Chow, D. W. Pack, P. Posocco, M. Fermeglia, S. Pricl and D. K. Smith, *Mol. Pharm*. 2011, **8**, 416-429; (*f*) S. P. Jones, G. M. Pavan, A. Danani, S. Pricl and D. K. Smith, *Chem. Eur. J*. 2010, **16**, 4519-4532; (*g*) P. Posocco, S. Pricl, S. Jones, A. Barnard and D. K. Smith, *Chem. Sci*. 2010, **1**, 393-404; (*h*) G. M. Pavan, A. Danani, S. Pricl and D. K. Smith, *J. Am. Chem. Soc*. 2009, **131**, 9686-9694; (*i*) P. Posocco, M. Ferrone, M. Fermeglia and S. Pricl, *Macromolecules*, 2007, **40**, 2257-2266.

22. S. E. Feller, Y. Zhang, R. W. Pastor, and B. R. Brooks, *J. Chem. Phys*. 1995, **103**, 4613-462.
23. J. Srinivasan, T. E. Cheatham III, P. Cieplak, P. A. Kollman and D. A. Case, *J. Am. Chem. Soc*. 1998, **120**, 9401-9409.
24. V. Tsui and D. A. Case, *Biopolymers* 2000, **56**, 275-291.